Jantke, Laura-Alice; Karttunen, Antti J.; Fässler, Thomas F.

Slicing Diamond for More sp^3 Group 14 Allotropes Ranging from Direct Bandgaps to Poor Metals

Published in:
ChemPhysChem

DOI:
10.1002/cphc.201700290

Published: 05/08/2017

Document Version
Early version, also known as pre-print

Final version:
Slicing Diamond for More sp3 Group 14 Allotropes Ranging from Direct Bandgaps to Poor Metals
Jantke, L. A.; Karttunen, A. J.; Fässler, T. F., ChemPhysChem 2017, 18, 1992–2006.
http://dx.doi.org/10.1002/cphc.201700290

Slicing Diamond for more sp^3-tetrel allotropes and group 14 frameworks reaching from direct to zero band gaps

Laura-Alice Jantke,[a] Antti J. Karttunen,[b] Thomas F. Fässler[a]

[a] L.-A. Jantke, Prof. Dr. T. F. Fässler
Department of Chemistry, Technische Universität München
Lichtenbergstr. 4, 85747 Garching (Germany)

[b] Prof. Dr. A. J. Karttunen
Department of Chemistry and Materials Science, Aalto University, 00076 Aalto (Finland)

Abstract

The large interest in novel Si allotropes has led to an intense investigation of tetrahedral framework structures during the last years. Recently, a guide to deriving sp^3-Si allotropes from atom slabs of the diamond structure enabled a systematic deduction of several low-density modifications. Some of the Si networks were recognized as experimentally known frameworks – so-called *chemi-inspired* structures. We herein present nine novel Si by modifying three-atom thick slabs of the cubic diamond structure after their smooth distortion by applying the same construction kit. The analysis of the structure-property relations of these frameworks with quantum chemical methods shows that several of them possess direct band gaps, which are in a range that is suitable for light conversion. The construction kit is also applied for the higher group 14 homologues Ge and Sn, revealing interesting differences for the band structures and relative energies of the homologues. A new semimetallic, zero-band gap modification of Sn is established.

Introduction

The properties of the tetrel elements silicon, germanium, and tin are mostly different from their smallest homologue carbon, on which all life on earth is based. Silicon, being the second most abundant element in Earth's crust, in contrast appears mainly as silicates, whereas almost all other Si compounds are man-made. The predominant modification of elemental silicon is α-Si, a semiconductor with an indirect band gap of 1.1 eV (room temperature)[1] and a large direct band gap of approximately 3.4 eV, which significantly limits the efficiency of silicon-based solar cells. Nevertheless, it is the most consistently studied element when it comes to semiconductors and the related industry.[2]

A study on the environmental impact of Si containing Li ion batteries confirms that this material could be used in sustainable product development,[3] even though α-Si suffers from a drastic volume change during charging/discharging cycles and may even crumble.[4] Consideration of these two important critical points – the poor energy conversion of α-Si in solar cells and its insufficient cycling stability when it is used as battery material – strongly drives the search for novel allotropes of this indispensable material. For the application as a Li ion battery material, low-density Si networks such as clathrates can be filled with guest atoms.[5] Other structures with networks of tetrahedrally interconnected Si atoms that form channels were recently proposed as a *chemi-inspired* structure based on the BSi_2 framework of $LiBSi_2$.[6] Even though the three-dimensional B/Si substructure constructed from five, six and seven-membered rings and revealing channels for the Li atoms looks rather complex, it was recently shown that the framework is a polytype that simply derives from the diamond structure.[7]

An important goal in the development of photovoltaic technology is to increase the efficiency of silicon solar cells and to reduce material consumption.[8] Computational studies in this field have yielded in novel tetragonal and other types of Si modifications with potential for photovoltaic efficiency improvements.[9] Another field of application for silicon is the use as thermoelectric materials,[10] which features low thermal conductivity together with a high electric conductivity. For silicon clathrate frameworks, it could be shown that the thermal conductivity is around one third of that of α-Si.[11]

In general, Si as well as Ge clathrates are objects of intense research over the last years, because they can be produced at ambient conditions and have outstanding properties.[12] Particularly theoretical chemistry and physics continuously deliver ideas for new Si allotropes and possible synthesis routes for experimental chemists; low-density Si allotropes are recently outlined in a

review article by Nolas *et al*.[5c] and Si phases useful for solar energy conversion by Wippermann *et al*.[13] Also the use of Si as a Li-ion battery anode material that is stable upon recharge and charge cycles pushes computational chemists to search for new allotropes.[14] Thereby, several theoretical approaches can roughly be distinguished. Many different approaches have been applied in the search for tetrahedral networks, for example, random search[15], swarm methods[16], genetic algorithm[17], or stacking of ring units[9b, 18]. When the unit cells get larger the computational cost for finding new structures drastically increases. Thus, alternative approaches to novel Si modifications are considered, such as taking advantage of structures derived for other materials such as carbon.[9a, 9d, 19] In addition the application of hierarchical structure principles leads to even more structure types as it has been successfully demonstrated for the clathrate structures. They were identified as duals of Frank-Kasper structures, which can be further modified to predict novel allotropes.[20] Furthermore, it could be seen that experimentally accessible clathrates are structurally similar to silica polymorphs and thus, the modification of zeolite structures is yet another strategy for discovering new structures.[15a] Another field that opens up in computational chemistry is the so-called inverse method of materials design that makes scientists search for materials after assigning specific properties.[21] For Carbon, it has been recently shown that the development of novel techniques might drastically decrease the computationally effort and opens up a huge field of novel element modifications expanding the possibilities as for example derived by a chemi-inspired approach.[22]

In our recent work, we described the systematic modification of the α-silicon structure by slicing it into slabs of three atoms that are smoothly modified and stacked again to result in networks with completely different properties. Since some of them were identified as (sub)structures of known binary and ternary intermetallics,[7] we named these structures possessing experimentally known frameworks with other element combinations *chemi-inspired* networks. Other than most structures derived from the cubic diamond modification,[23] the here constructed networks do not conserve structure features thereof and are thus not likely to rearrange immediately to the α-silicon network. Also the realization of predicted structures in experiment[24] gives us confidence that integrating the work towards new carbon and silicon allotropes might produce very interesting promising structures in the future.

The two higher group 14 homologues germanium and tin both have a cubic allotrope analogous to α-silicon. At ambient conditions, α-Ge is the thermodynamically favored form of Ge, while for Sn the metallic β-Sn allotrope is the thermodynamically favored modification. The low

temperature modification α-Sn is a powdery grey solid that transforms to β-Sn at 13.2° C. The two tetrels Si and Ge in contrast need high pressure of about 11 GPa to transform into their β-modification, while the α-modification is stable at ambient conditions. For all three elements Si, Ge, and Sn, we consider here novel tetragonal sp^3-networks that might promote also the acquisition of a material that can satisfy today's demand in renewable energy sources. The band gap of the α modifications of the heavier tetrels continuously decreases going down the periodic table from Si having an indirect band gap, to Ge with direct and indirect gap at almost equal sizes, and Sn being a semi metal with zero band gap. Thus studying the novel derived allotropes also for Ge and Sn will allow a better comparison of their properties as well. Fan *et al*. recently started to include alloys for their computational studies on new modifications, for example Si/Ge alloys;[25] a consideration that would also be very interesting for our structures, as the element structures introduced as *chemi-inspired* Si allotropes have a counterpart in experimentally accessible substructures of ternary phases.[7] Examples of those are more frequent among the higher homologue Sn together with other elements such as Ga and Zn. The stability of the directly connected element structures can thus be compared to the substructures in intermetallics.

Computational Details

All structures were modeled following the procedure described in the construction part of the recent publication of Jantke *et al*.[7] The resulting structures were first optimized with the CRYSTAL09 program package[26] using the Perdew-Burke-Ernzerhof (PBE) DFT-functional[27] for the exchange and correlation parts and a modified split-valence + polarization basis set for Si, Ge, and Sn[28]. For Ge and Sn, scalar relativistic effective core potential is applied for 10 and 28 core electrons, respectively. Both the lattice and atomic parameters were allowed to relax without any symmetry restrictions (feasible in space group *P*1 (No. 1)). The initial cell parameters are $a = b =$ 7.6805 Å and c = 9.7758 Å, all angles being 90°. The shrinking factor (SHRINK) to determine the density of the Monkhorst-Pack type k-mesh is 4 for each spatial direction generating 16 to 20 k-points in the irreducible part of the Brillouin zone. Tight tolerance factors of 7, 7, 7, 7, 14 were used for the evaluation of the Coulomb and exchange integrals (TOLINTEG). Default optimization convergence thresholds and large integration grid (LGRID) for the density functional part were applied in this first optimization. The symmetry of the optimized structures was determined with FINDSYM[29] at a tolerance of 0.1. The structures were re-optimized in the resulting space group using the Perdew-Burke-

Ernzerhof hybrid functional (DFT-PBE0)[27, 30], while the structure was able to relax both the lattice and atomic parameters within the constraints given by symmetry. The shrinking factors are 8 for each special direction generating a mesh of 75 to 170 k-points in the irreducible part of the Brillouin zone. For this second step, tighter tolerance factors of 8, 8, 8, 8, 16 for the Coulomb and exchange integrals were applied, as well as default optimization thresholds and extra-large integration grids (XLGRID) for the density functional part. The local minimum character of all structures was confirmed with frequency calculations.[31] For the calculations of the band structures, the properties package of CRYSTAL09 was used. After finding the optimal path in the irreducible part of the Brillouin zone[32], the structure was investigated with 400 *k*-points along the path. The natural tiling[33] of all networks was determined using the TOPOS4.0 program package[34].

The relative energy corresponds to the difference in total energy between the discussed network and the α-modification of the respective element. Ii is further referred to one atom; thus the total energy of the given network is divided by the number *n* of atoms per unit cell (Equation 1).

$$\Delta E_{net} = \frac{E_{net}^{total}}{n} - \frac{E_{\alpha}^{total}}{2} \quad (1)$$

Results and Discussion

Schematic construction of novel polytypes of three-atom slabs

The three atom thick layer cut out along the [110] face of the cubic diamond structure (Figure 1a) consists of four-bonded (*4b*) and two-bonded (*2b)* atoms. The *4b* atoms span a plane with *2b* atoms lying below (*L*) and above (*U*) this plane (Figure 1b). Distortions of the resulting eight-membered rings according to Figure 1c connect *2b* atoms within the layer and the resulting *3b* atoms are capable to connect the layers in perpendicular direction. Distortions are possible within the wrinkled eight membered ring forming a pair of five membered rings (hump and dell with the bond above or below the plane, respectively). Crosswise connection of two bonds creates a realgar-type unit. Forming exclusively bonds to neighboring atoms outside of the ring retains the eight-membered ring. Based on this principle, we introduced in an earlier publication Layer A with a Cairo (pentagonal) tiling (Figure 2) [7, 35] and Layer B_a (named Layer B in the earlier publication [7]), which served for the construction of several *chemi-inspired* polytypes.

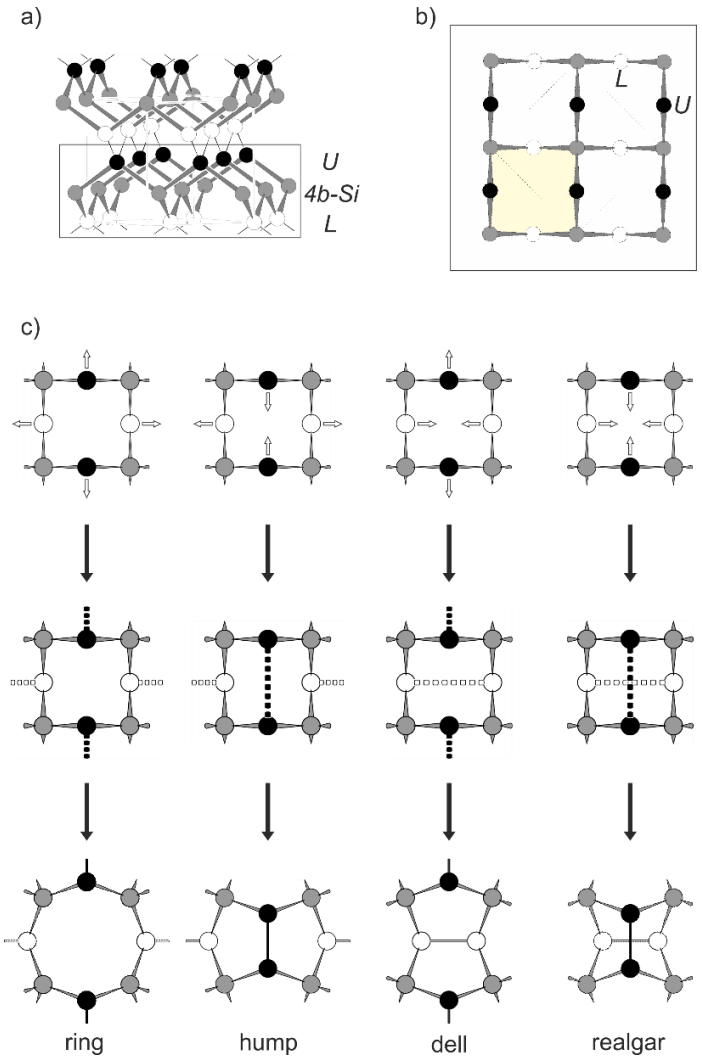

Figure 1. Distortions of the three-atom thick cutout from the cubic diamond modification. a) The box represents a three-atom thick cutout of α-Si creating two-fold connected surface Si atoms on top (U, black spheres) and below (L , open spheres) the plane through four-fold connected atoms (grey spheres). b) The top view of one such layer representing a 2×2 superstructure of the central unit (highlighted in yellow) used as repeating unit for all modeled networks. c) Modifications of the single rings by four different distortions.

In this work, we define a set of layers which allows to construct another nine structures (Figure 2). The connection of two-bonded atoms within the layer can either be distributed alternately to result in the Cairo tiling of layer A, or contain realgar-type units that alternate with eight-membered rings (layer C). Mixing of the two motifs leads to layer B_a,[7] and the permutations B_b and $B_{b'}$. B_b and $B_{b'}$ are superimposable by a horizontal mirror plane.

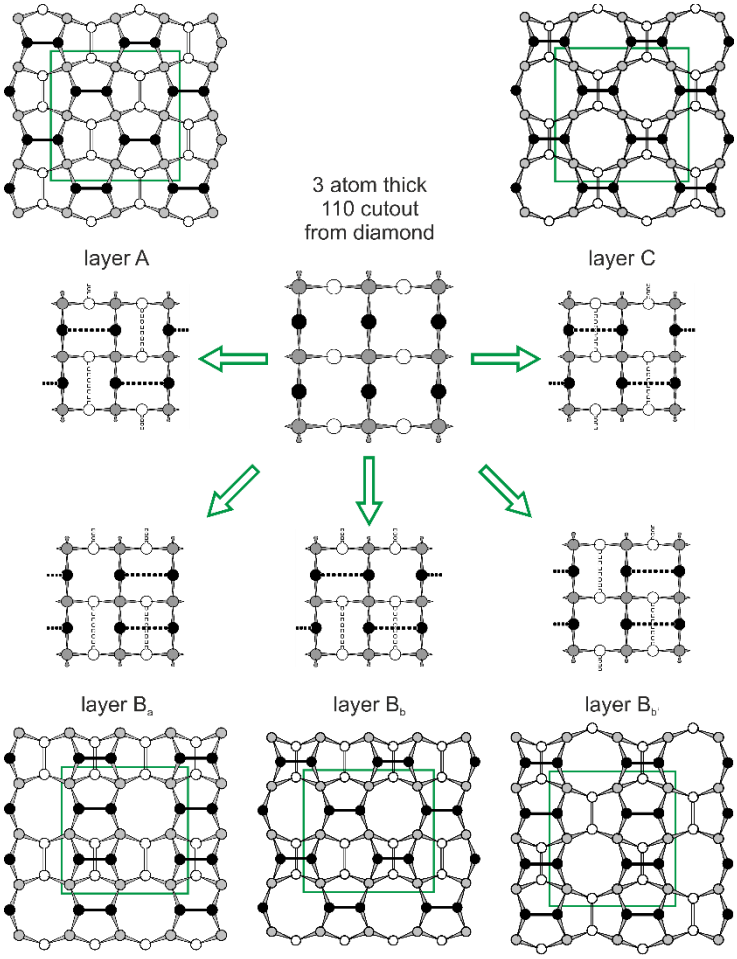

Figure 2. Five atom layers A, B_a, B_b, $B_{b'}$, and C resulting from distortion of the three-atom thick section of the diamond structure shown in the center of the figure. Types of distortion are shown in Figure 1.

In a second step the layers are stacked so that all three-bonded atoms of adjacent layers form a covalent bond between the layers to result in tetrahedral three-dimensional frameworks. Such a construction is easily realized by shifting and rotating the layers with respect to each other. The superscript "*" denotes a rotation and the superscripts 1 to 6 a translational shift within the layer plane as given in the legend of Table 1. Following this rather construction steps by simply stacking solely two layers arises in nine novel structures, which can easily be related to each other and still each gets a very unique set of properties.

Table 1. Structures **1** – **9** by a two slab stacking sequence of atoms slabs A, B_a, B_b, B_c, and C. The superscript * denotes a 90° in plane rotation of the layer, superscript numbers 1 to 6 shift vectors according to the unit cell given in Figure 2: 1 (0.25, 0.25), 2 (0.5, 0), 3 (0, 0.5), 4 (0.5, 0.5), 5 (0.75, 0.25), and 6 (0.25, 0.75).[7] Pearson symbol, space group (no.), and the natural tiling are listed. The formula for the natural tiling also contains the numbers of symmetry independent tiles, not only the ratio of different tiles. Networks **1**−**3** are built of layers B_b and/or B_b'; networks **4** and **5** are constructed using layer C and networks **6**–**9** are the result of a combination of different layers.

No.	Name[34]	Stacking Sequence	Pearson Symbol	Space Group (no.)	minimal ring size	maximal ring size	average ring size	Natural Tiling
1	**tum5**	$B_b\,B_c$*	*oP*24	*Pmma* (51)	5	7	6	$[5^4] + 2[5^2.7^2] + [7^4] + 4[5^2.6^2.7^2]$
2	**tum6**	$B_b\,B_b^1$	*mP*24	$P12_11$ (4)	5	8	6	$[8^3] + [5^4] + [5^2.8^2] + [5^2.8^3] + [5^6.8^2] + [5^{10}.8^2]$
3	**tum7**	$B_b\,B_b$*	*oP*24	*Pmm*2 (25)	4	7	6	$2[5^4] + [5^6.6^4.7^2] + [5^4.6^4.7^4] + [4^2.5^8.6^4] + [4^2.5^6.6^4.7^2]$
4	**jfk1**	$A\,B_a^2$*	*tP*24	*Pmm*2 (25)	4	7	5.47	$[5^4] + [5^2.7^2] + [5^6.6^4.7^2] + [5^4.6^4.7^4] + 2[4^2.5^8.6^4]$
5	**jfk2**	$B_b\,A^2$*	*oP*24	*Pmm*2 (25)	4	7	5.77	$[5^4] + 4[5^2.7^2] + 4[5^2.6^2.7^2] + [5^4.6^4.7^4] + [4^2.5^8.6^4]$
6	**jfk3**	$A\,C^1$	*tP*12	$P\bar{4}$ (81)	5	8	6.56	$2[8^3] + [5^4] + 10[5^2.8^2]$
7	**jfk4**	$C\,B_a^4$	*oC*48	*C*222 (21)	5	8	6.15	$2[8^3] + 3[5^4] + 2[5^2.8^2] + 4[5^2.8^3] + 4[5^6.8^2]$
8	**alt1**	$C\,C^1$	*oC*12	*C*222 (21)	5	8	6.62	$2[8^3] + [5^4] + 4[5^2.8^2]$
9	**alt2**	C C*	*tP*12	$P4_2/nnm$ (134)	5	7	6	$[5^4] + [7^4] + 2[5^2.6^2.7^2]$

[1]) The symbol specifies the Bravais lattice by two (italic) letters (with lower case letter for the crystal system and the upper case letter for the lattice type), the number corresponds to the number of atoms in the unit cell.

The structure of tum5 (1) in comparison to tum1

We illustrate the strength of our systematic structure search with the help of the tetrahedral network **tum5** (**1**) and its close relation to **tum1** (Figure 3). The latter structure appears in the experimentally known $BiSi_2$ framework of $LiBSi_2$[36] in which B is substituted by Si and in the covalent sub-structure of $Na_5T_{2+x}Sn_{10-x}$ (T = Hg, Zn; $x \approx 0.5$)[37] with T substituted by Sn. Thus this frameworks has been branded as a *chemi-inspired* Si allotrope[7].

The combination of B_a and B_a* results in known **tum1** (Figure 3a), whereas combining layer B_b with $B_{b'}$* arises in the new structure **tum5** (**1**, Figure 3b). The change from the basic layers of **tum1** to those of **tum5** is highlighted with solid and dashed lines in Figures 3a and 3b – the solid lines refer to bonds that are formed in the appropriate structure, while the dashed lines refer to bonds of the other structure, which are broken due to the reorganization of the layers. Such a reconstruction of atoms within a layer was described before in an experimentally observed equivalent framework: Structures **unj1** and **unj2**[7] show both helical channels running in parallel (**unj1**) or perpendicular (**unj2**) to each other. The analogue transformation of atoms appears in the experimentally established phase transition of the two modifications of Na_2ZnSn_5.[35] Such smooth rearrangements may lead to several promising element modifications, as it is computationally shown also for boron networks based on shifts of the B_{12} units that serve as building blocks there.[9e]

Structure **1** can be described in space group *Pmma* (51) with 5 symmetry independent atom positions per unit cell.[38] Both structures, **tum1** and **tum5** have the same tiling in $[5^4] + 2[5^2.7^2] + [7^4] + 4[5^2.6^2.7^2]$ polyhedra, but a closer analysis discloses that **1** bears two different sorts of $[5^2.6^2.7^2]$ tiles; one with the two five membered rings (and the two seven membered rings) directly connected (blue in Figures 3c and d) and one, where those are exchanged (green in Figure 3d). The known framework **tum1** has only the first tile. In order to distinguish between them, we marked the latter with an asterisk and the more detailed writing of the natural tiling for structure **1** is consequently: $[5^4] + 2[5^2.7^2] + [7^4] + 2[5^2.6^2.7^2] + 2[5^2.6^2.7^2]$*.[39]

The differences in strain and relative energy of **tum1** and **tum3** have been described before, [7] by the different relative positions of the larger unities ($[5^4] + 4[5^2.6^2.7^2]$). The same is observed here and the ($[5^4] + 4[5^2.6^2.7^2]$) unities share one face for **tum1** (Figure 3e), whereas the ($[5^4] + 2[5^2.6^2.7^2] + 2[5^2.6^2.7^2]$*) unities share two faces for **tum5** (Figure 3f).[40] The topological analysis of **1** is identical to this of **tum1** with an average ring size of 6 and a ratio of faces per tile that is 5.

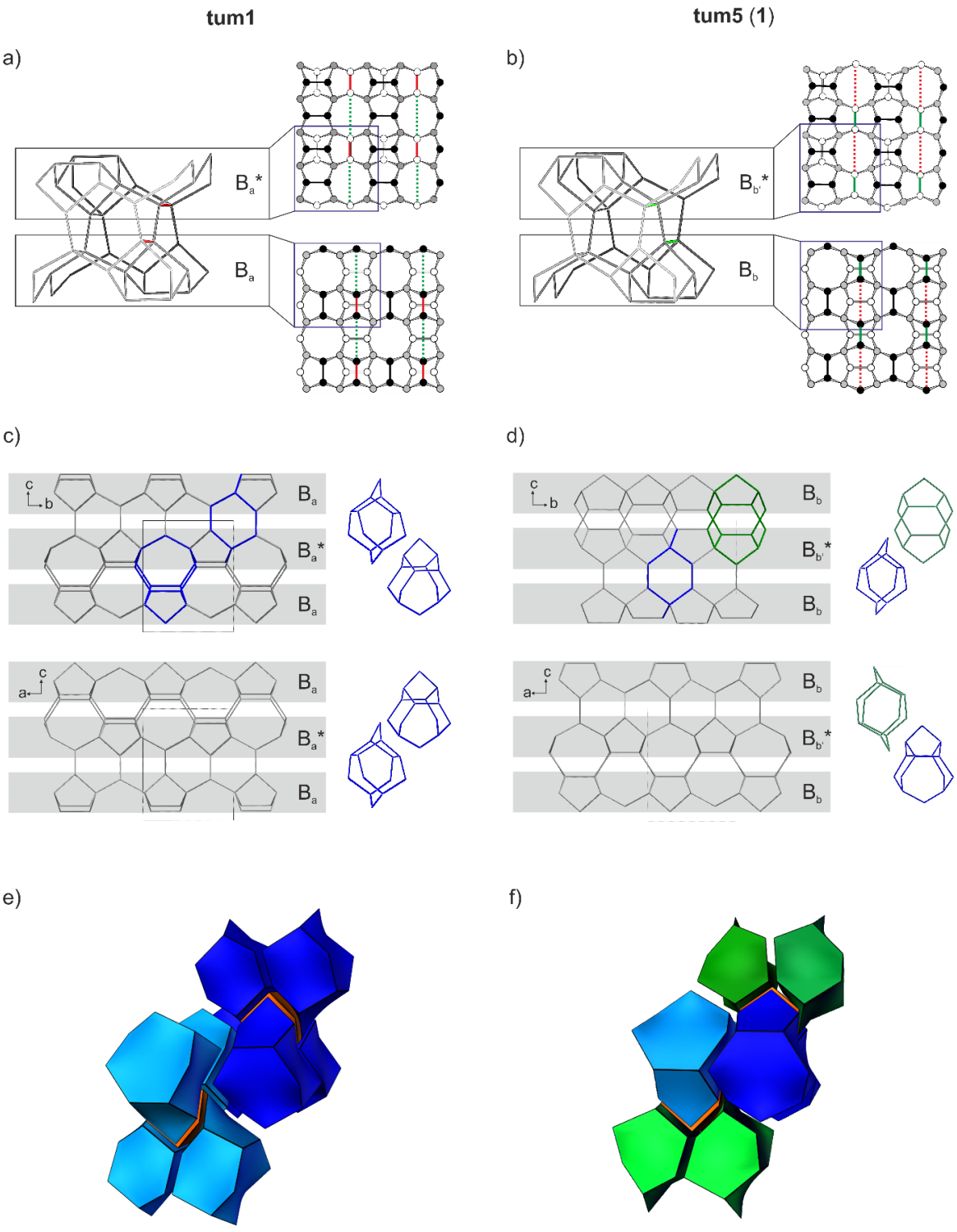

Figure 3. A comparison of structures **tum1** and **tum5** (**1**). a) and b) Stacking of the layers to result in structures **tum1** and **tum5**; the change of only two parallel running bonds (red for **tum1** and green for **tum5**) leads to a new structure with completely different properties. c) and d) Parallel projections and stacking sequences of **tum1** (c) and **tum5** (d). The tiles, which are aligned to result in the channel like systems are shown next to the appropriate projections. Tile $[5^2.6^2.7^2]$ is shown in blue and tile $[5^2.6^2.7^2]$* in green, respectively. e) and f) The larger unity consisting of ($[5^4]$ + $4[5^2.6^2.7^2]$) tiles for **tum1** (e) and of ($[5^4]$ + $2[5^2.6^2.7^2]$ + $2[5^2.6^2.7^2]$*) units for **tum5** (f) and their relative positions to each other. The upper and lower unities are colored in dark and light blue and green, respectively, even though they are symmetry dependent.

Electronic properties of** tum5 **(1) – a tetrel allotrope with promising properties

After constructing the networks and subsequently optimizing their structures for the three homologues Si, Ge, and Sn, the structural analysis of **1** for **1-Si, 1-Ge** and **1-Sn** reveals bond ranges, angles and relative atomic volumes that are comparable to those of **tum1** (Figures 5–7 and Table 3).

Even though the networks are closely related, the quantum chemical analysis shows significant differences: The relative energy of **1** is 13.8 kJ/mol, 12.7 kJ/mol and 4.1 kJ/mol for **1-Si**, **1-Ge**, and **1-Sn**, respectively, whereas those of **tum1** arises to 9.8 kJ/mol, 9.3 kJ/mol and 7.6 kJ/mol for **tum1-Si**, **tum1-Ge**, and **tum1-Sn**, respectively. Thus the higher homologues Si and Ge energetically prefer the **tum1** structure, whereas the Sn allotrope has a lower energy adapting the network **1 (tum5)**.

The analysis of the band structures shows a smaller band gap for **1** (1.39 eV, 0.44 eV and 0.00 eV for **1-Si**, **1-Ge**, and **1-Sn**, respectively) than for **tum1** (2.53 eV, 1.43 eV, and 0.73 eV for **tum1-Si**, **tum1-Ge**, and **tum1-Sn**, respectively). Moving from Si to Ge has a drastic influence on the conduction bands (Figure 4) and the Ge network **1-Ge** in contrast to **1-Si** is a *direct band gap semiconductor*. In **1-Sn** valence and conduction band touch and a semimetal (zero band gap) is formed. The **tum1** structure in contrast is a semiconductor with indirect band gap for all three elements (the band structures of all considered structures are represented in the Supporting Information). A similar trend in the band structure is also reported for the α-modifications of Si, Ge and Sn.

Notably, structure **pbam** recently described by Mujica *et al.*[23b] also fits in the described polytypes as it also shows this set of a seven-membered ring channels neighboring five-membered rings resulting in a $[5^2.6^2.7^2]$ tile (blue tile in Figure 3). However, **pbam** cannot be derived by the here presented kit. Furthermore, as expressed by the natural tiling $[5^2.6^2] + 2[6^4] + [6^2.7^2] + [5^2.6^2.7^2]$, **pbam** shows that the adamantine-type $[6^4]$ tile, which is the only unit in the α-modification, persists. The high abundance of this building block in **pbam** explains the low total energy of 3.97 kJ/mol when recalculated at the same level of theory. Thus **pbam** represents a modification that simply retains a larger part of the diamond structure.

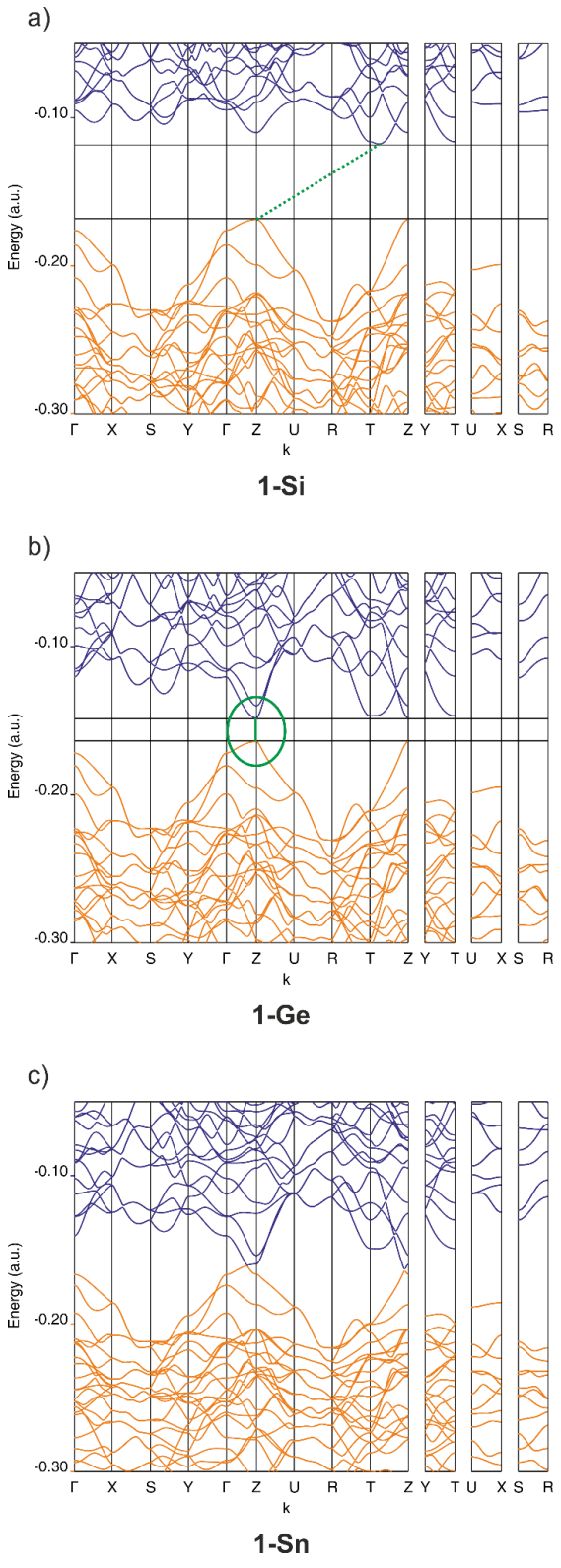

Figure 4. Band structures for network **1** of the three homologues Si, Ge, and Sn. The path is chosen according to the work of Curtarolo et. al.[41] a) **1-Si** is a semiconductor with an indirect band gap of 1.39 eV. b) **1-Ge** is a semiconductor with a direct band gap of 0.44 eV. c) In **1-Sn** a zero band gap appears along the path between Γ and Z. The conduction and valence bands are colored blue and orange, respectively. To guide the eye, the band the maximum of the valence bands is connected to the minimum of the conduction bands with a green line and for Ge also with a green circle.

Topological analysis of several structures build of layers A, B_a, B_b, $B_{b'}$, and C

Similar to **tum5** discussed above, nine other structures, which can be seen as simple polytypes of the diamond structure, are introduced in this work (Table 1). As their basic layers all comprise of realgar units, structures **tum1**–**tum4**[7] are included in the topological, structural and computational analyses.

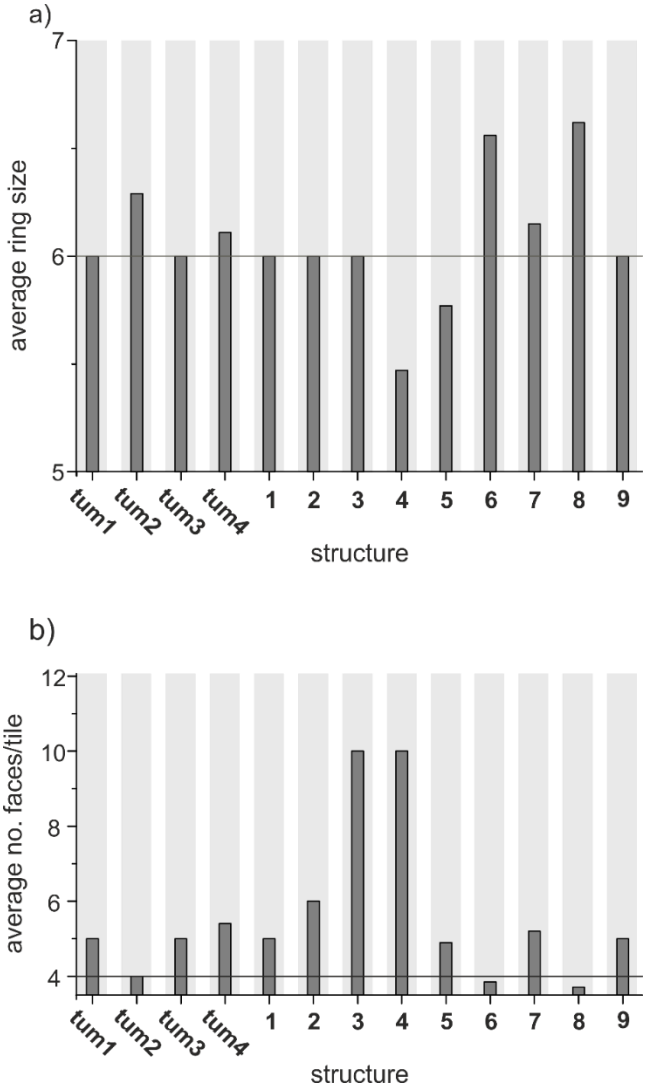

Figure 5. Topological parameters of the considered networks **1**–**9** as well as **tum1**–**tum4**.[7] a) Average ring size resulting from the natural tiling of the structures.[33a] The line indicated the average ring size 6 for the diamond structure type (natural tiling in [6^4]). b) Average ratio of faces per tile. The line represents the ratio four of the diamond structure type. The bars referring to structures that contain realgar units are highlighted in grey, the others not.

In order to geometrically analyze the structures independent on the atoms size and thus independent of the element(s), we use the parameters ring size (Figure 3a) and the ratio of faces per tile (Figure 3b). The natural tiling introduced by O'Keeffe et al.[33a] defines natural tiles

with rules that comprise – among others – that so-called *strong rings* are considered or with other words rings that are not the sum of any number of smaller cycles.[42]

The average ring sizes range from 5.47 to 6.62 for **4** and **8**, respectively (Figure 5a). The ring sizes for the strong rings of our tetrahedral networks range from four (planar four membered ring between two adjacent realgar units in stacking direction) to eight (e.g. the wrinkled ring within the basic layers, Table 1). The ring size is, especially if the rings get smaller than six membered as it is seen for the cubic diamond modification (tiling in $[6^4]$), a parameter that refers well to the bond strain within a network.

The ratio of faces per tile (Figure 5b) is rather a measure of the polyhedra size and ranges from 3.71 (**8**) to 10 (**3** and **4**). Interestingly, only two networks of our set have a face/tile ratio that is smaller than four found for the α-modifications. The structures **6** and **8** both show the same natural tiles $[8^3]$, $[5^2.8^2]$, and $[5^4]$, but differently composed.

Structural and computational analysis of nine considered structures together with the chemi-inspired *structures tum1–tum4 as modifications of the three elements Si, Ge, and Sn*

The nine considered tetrahedral three-dimensional framework structures together with the *chemi-inspired* diamond polytypes described before [7] were optimized at the DFT-PBE0/SVP level of theory as element modifications of Si, Ge and Sn (unit cell coordinates are listed in the Supporting Information).

The structural characteristics minimal and maximal bond length (Figure 6a), smallest and largest angle (Figure 6b) as well as the relative atomic volume (Figure 6c) are dependent on the considered element. However, the range from smallest to largest bond, the angles and the relative atomic volumes (in terms of fractions of the atomic volume of the considered α-modifications) vary only slightly from Si to Sn (Figure 6). One exception is structure **6** that has a significantly smaller range for the bond lengths for Ge than for the other elements, which is however not influencing other results (Figure 6a).[43]

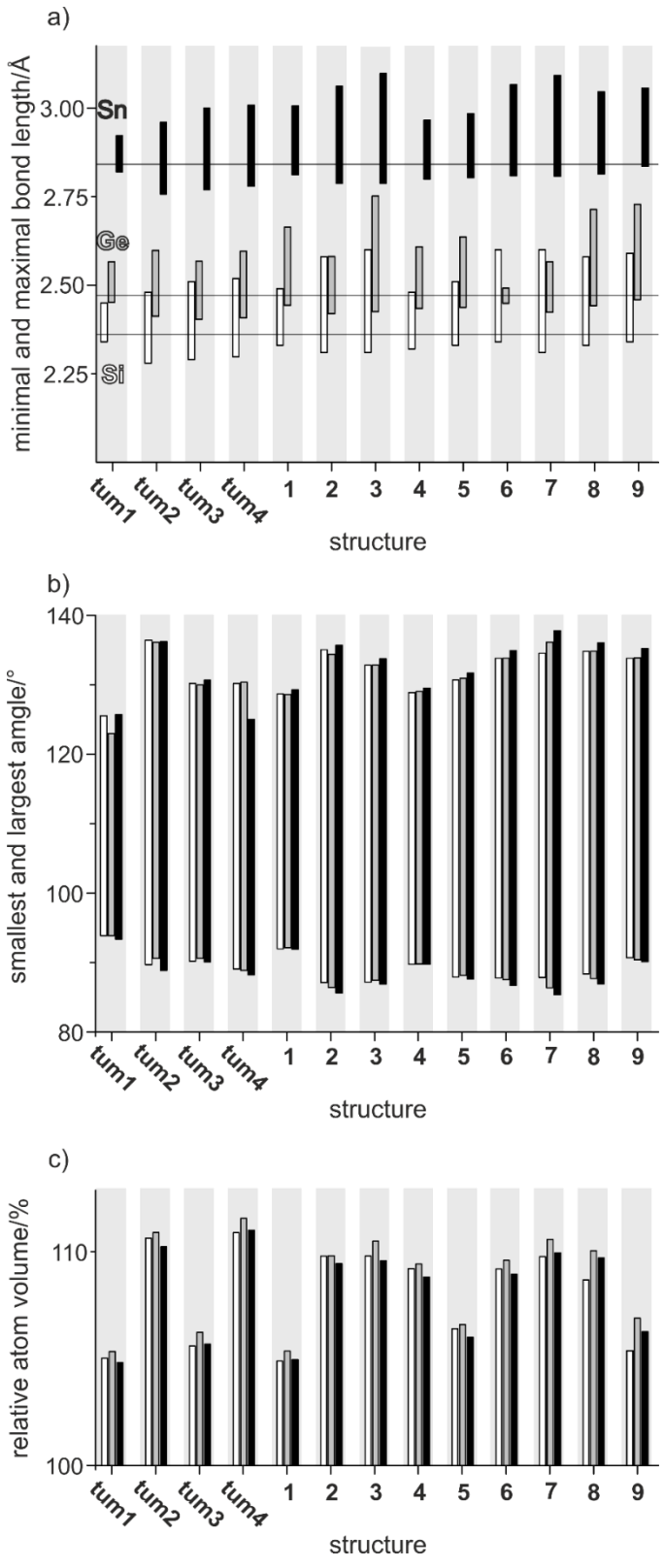

Figure 6. Structural parameters of all considered tetrahedrally connected networks. White, grey and black bars refer to Si, Ge, and Sn, respectively. a) Shortest and longest bond length. The values of the α-modifications calculated at the same PBE0/SVP level of theory (2.36 Å for Si, 2.48 Å for Ge, and 2.81 Å for Sn) are shown as lines. b) Range between smallest and largest appearing bond angle. c) Relative atom volume based on the calculation value of atomic volume (considered structure) / atomic volume (calculated α-modification).

The relative energies as compared to the respective α-modifications decrease for all structures with the order of the elements Si, Ge and Sn (Figure 7). In a qualitative description, the heavier elements allow for a larger flexibility with regard to the bond strain and the deviation from the ideal tetrahedral angle, which originates from the more diffuse character of the respective atomic orbitals.

The calculated values range for Si from 9.8 kJ/mol (**tum1-Si**) to 31.3 kJ/mol (**8-Si**), for Ge the networks show relative energies between 9.3 kJ/mol (**tum1-Ge**) and 28.3 kJ/mol (**8-Ge**), and for Sn values between 4.1 kJ/mol (**1-Sn**) and 22.9 kJ/mol (**8-Sn**) were obtained. Thus, the *chemi-inspired* network **tum1**, which is experimentally found as a substituted Si framework,[36] shows for Si a comparably smaller relative energy than for Sn, even though it exists also as a Zn/Sn or Hg/Zn network in $Na_5T_{2+x}Sn_{10-x}$ with this topology.[37] But for the latter, the relative energy of structure **1** lies among the accessible networks. Note that for Si modifications, the relative energy of **tum1** is also lower than that of networks only found as substituted Sn structures (e.g. **unj1** and **unj2**), whereas for Sn, **tum1** has a higher relative energy than the structures without realgar units.

The DFT-PBE0 functional is known to overestimate the band gaps and therefore, we recalculated the α-modifications that reveal a gap of 1.87 eV (instead of 1.17 eV at 0 K or 1.12 eV at room temperature[1], respectively) for Si and 0.83 for Ge; α-Sn shows a zero-gap. If all calculated band gaps for Si are corrected for the difference of $\alpha\text{-Si}^{PBE0}$ and α-Si[2], five of the resulting direct band gap compounds that are listed in Table 2 and possess the optimal range of 1.5 eV that is suitable for sunlight conversion. For a more detailed insight, the band structures are shown in the Supporting Information.

Semiconducting Si networks can be doped, which changes the relative position of the Fermi-level and thus increases the electric conductivity. It is known that a doped semiconductor with more than one minimum get more efficient, as more electrons populate the conduction band at a time. For this reason, all herein considered Si structures are also interesting candidates for other semiconductor applications such as thermoelectrics. The doping of Si in such high content that atoms at one Wyckoff position were substituted led to the structure $LiBSi_2$[36] that has a B/Si substructure identical to **tum1** and can serve as a host for Li ions that are situated in channels, a promising situation for battery materials.

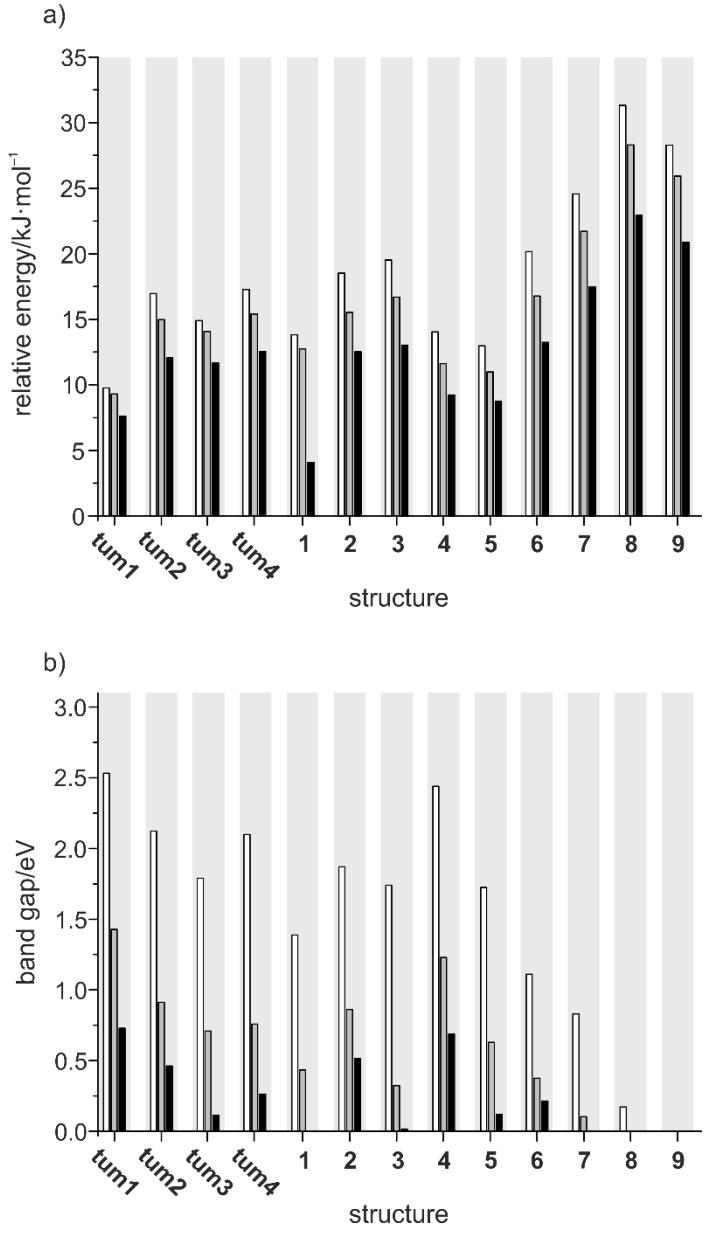

Figure 7. The electronic properties of all considered structures. a) Display of all relative energies in kJ/mol based on the α-modification of the corresponding element. The comparison is based on one atom, thus the energy of the unit cell is divided through the atoms filling it. b) Band gaps of all considered networks. The diagram is always showing the smallest gap, independently from its character. The element modifications are shown in black, grey, and white for Si, Ge, and Sn, respectively. The bars referring to structures that contain realgar units are highlighted in grey, the others not.

Table 2. Computational Analysis of all considered structures. The total energies of the optimized networks are displayed with respect to the α-modification (0.0 kJ/mol) of each element. Further, the band gap, which is labeled with (d) if it is a direct one, the direct band gap, and for Si the corrected direct band gap, are listed for each tetrel element. The correction factor for the direct band gap is the difference between the DFT-PBE0/SVP (indirect) band gap of α-Si and the experimental band gap of α-Si[1].

	E_{rel}/kJ•mol^{-1}			band gap/eV	band gap^{direct}/eV	band gap$^{dir,\ corr}$/eV	band gap/eV	band gap^{direct}/eV	band gap/eV	band gap^{direct}/eV
	Si	**Ge**	**Sn**	**Si**			**Ge**		**Sn**	
α	0.0	0.0	0.0	1.87	3.95	3.20	0.83 (d)	-	0.00	-
tum1	9.8	9.3	7.6	2.53	2.59	1.84	1.43	1.54	0.73	0.87
tum2	17.0	15.0	12.1	2.12	2.35	1.60	0.91	1.12	0.46	0.63
tum3	14.9	14.1	11.7	1.79	1.99	1.24	0.71 (d)	-	0.11	-
tum4	17.3	15.4	12.6	2.10	2.03	1.28	0.76 (d)	-	0.26	-
1	13.8	12.7	4.1	1.39	1.74	0.99	0.44 (d)	-	0.00	-
2	18.5	15.5	12.5	1.87	2.18	1.43	0.86	1.35	0.51	0.89
3	19.5	16.7	13.0	1.74 (d)	-	0.99	0.32 (d)	-	0.02 (d)	-
4	14.0	11.6	9.2	2.44	2.58	1.83	1.23	1.28	0.69	0.73
5	13.0	11.0	8.8	1.72	2.26	1.51	0.63 (d)	-	0.12	0.13
6	20.2	16.8	13.2	1.11	2.44	1.69	0.38	0.71	0.21 (d)	-
7	24.6	21.7	17.5	0.83	1.30	0.55	0.11	0.48	0.00	0.17
8	31.3	28.3	22.9	0.17	3.20	2.45	0.00	1.03	0.00	0.03
9	28.3	25.9	20.9	0.00	1.50	0.75	0.00	0.00	0.00	-

Structure description of the networks 2–9

In addition to structure **1**, the other eight structures also bear several interesting properties and it is likely to find some of them in binary or ternary phase systems. For an easy identification of measured X-Ray data, we included the theoretical powder diffractograms for all nine structures as Si element modifications in the Supporting Information.

tum6 (2). Stacking of layers B_b and B_b^1 results in the four-connected network **tum6** (**2**). The two-layer stacking (Figure 8a) is described in space group $P12_11$ (4) with eleven symmetry independent Si atoms in the unit cell.[44] Network **2** has a natural tiling with $[8^3]$ + $[5^4]$ + $[5^2.8^2]$ + $[5^2.8^3]$ + $[5^6.8^2]$ + $[5^{10}.8^2]$ polyhedra. Comparing the tiling, tile $[5^2.8^2]$ that is the only tile, structures **unj1**, **unj2**, and **unj3** consist of and is stacked following a screw for those,[7] is here aligned in turns with $[8^3]$ (violet in Figure 8b) along the *ac* diagonal which all $[5^2.8^2]$ aligned in parallel. In between, the screwed $[5^{10}.8^2]$ polyhedron (yellow in Figure 8c), is sitting.

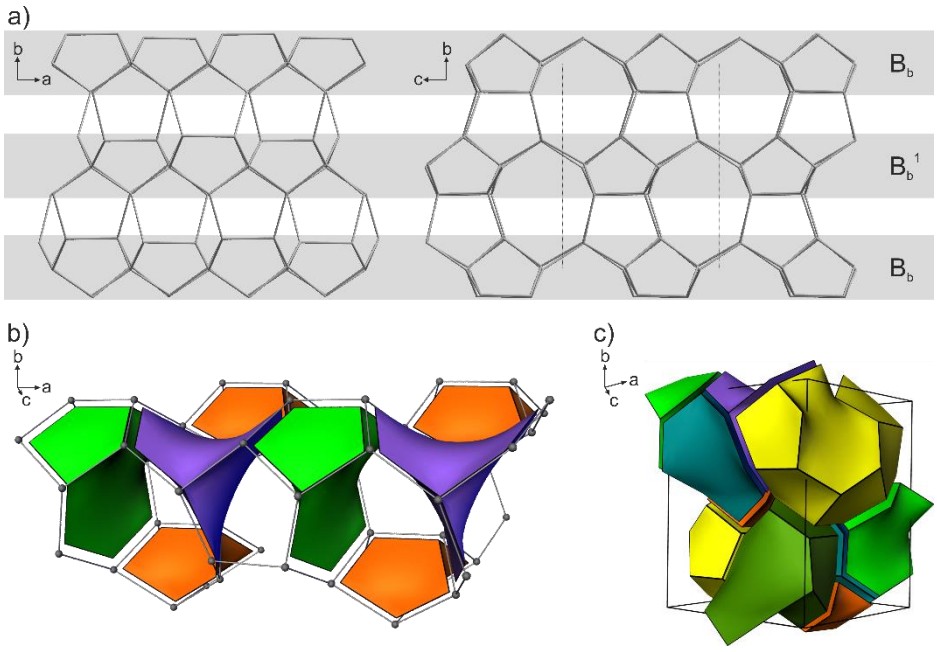

Figure 8. The network of structure **tum6** (**2**). a) Parallel projection on the stacking sequence along the c and the a axis, respectively. b) Representation of the alignment of the smaller natural tiles $[5^2.8^2]$ (green), $[5^4]$ (orange) and $[8^3]$ (purple). c) Filling of the unit cell in terms of natural tiles; the tiling is $[8^3]$ (purple) + $[5^4]$ (orange) + $[5^2.8^2]$ (green) + $[5^2.8^3]$ (turquoise) + $[5^6.8^2]$ (forest green) + $[5^{10}.8^2]$ (yellow).

tum7 (3.) Stacking layer B_b and layer B_b^* results in structure **3** that can be described in space group *Pmm*2 with ten symmetry independent Si positions in the unit cell (Figure 9a). The natural tiling of this structure is $2[5^4]$ + $[5^6.6^4.7^2]$ + $[5^4.6^4.7^4]$ + $[4^2.5^8.6^4]$ + $[4^2.5^6.6^4.7^2]$ (Figure 9b).

In contrast to networks constructed with other layers than B_b or combinations of B_b with different layers, structures **2** and **3** offer large cages and are therefore possible candidates for intercalation materials.

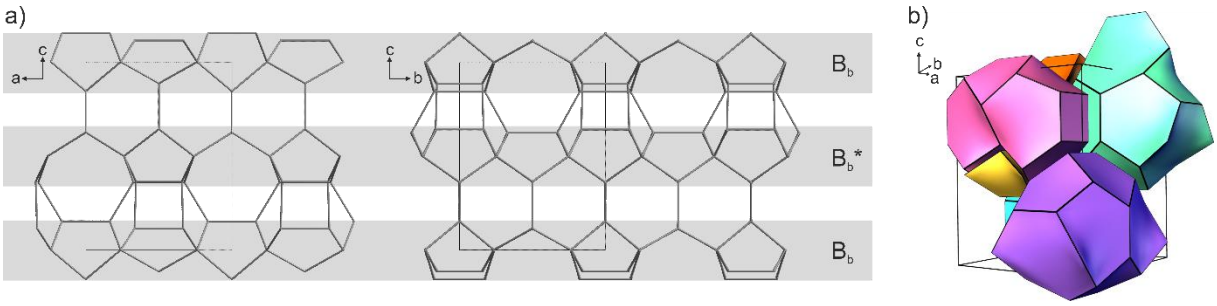

Figure 9. Representation of network **3**. a) Parallel projection and stacking sequence B_bB_b* along directions b and a, respectively. b) Filling of the unit cell in terms of natural tiling in 2[5^4] (orange and yellow) + [$5^6.6^4.7^2$] (purple) + [$5^4.6^4.7^4$] (turquoise) + [$4^2.5^8.6^4$] (pink) + [$4^2.5^6.6^4.7^2$] (light blue).

jfk1 (4). After discussing the set of *chemi-inspired networks* that can be constructed by stacking layer A and layer B_a, but never by the combination of these two, we included one structure resulting from the combination of A with B_a^2*. Structure **jfk1** (**4**) can be described in space group *Pmm*2 (25) with ten symmetry independent Si positions per unit cell (Figure 10a). It shows a natural tiling in [5^4] + [$5^2.7^2$] + [$5^6.6^4.7^2$] + [$5^4.6^4.7^4$] + 2 [$4^2.5^8.6^4$] polyhedra resulting in the smallest average ring size of all herein discussed networks of 5.47 (Figure 10b). The network is bearing large tiles with obtuse angles and the same large average face per tile number of 10 like **tum7** (**3**) making it a possible candidate for intercalation materials. Between the large tiles, the [$5^2.7^2$] tile fits in and allows the structure for more relaxation compared to **3**. Structure **4** has thus a smaller relative energy.

jfk2 (5.) Stacking layers C and A^{2*} arises in network **5**, which is described in space group *Pmm*2 (25) with ten symmetry independent Si sites per unit cell (Figure 10c). Its natural tiling is [5^4] + 4 [$5^2.7^2$] (all symmetry independent) + 4 [$5^2.6^2.7^2$]* (two pairs of symmetry independent tiles) + [$5^4.6^4.7^4$] + [$4^2.5^8.6^4$] (Figure 10d). This structure includes various above described features; it bears large tiles with obtuse angles, but also the tile [$5^2.6^2.7^2$]*, which is covering two faces of the realgar unit; the other two faces are neighboring to the [$4^2.5^8.6^4$] tile. The other pair of [$5^2.6^2.7^2$]* tiles has no shared face with a realgar unit, but with the large [$4^2.5^8.6^4$] tile. The parallel projection along the *a* axis is similar to the one of **4** and along the *b* axis, it is identical to **1**.

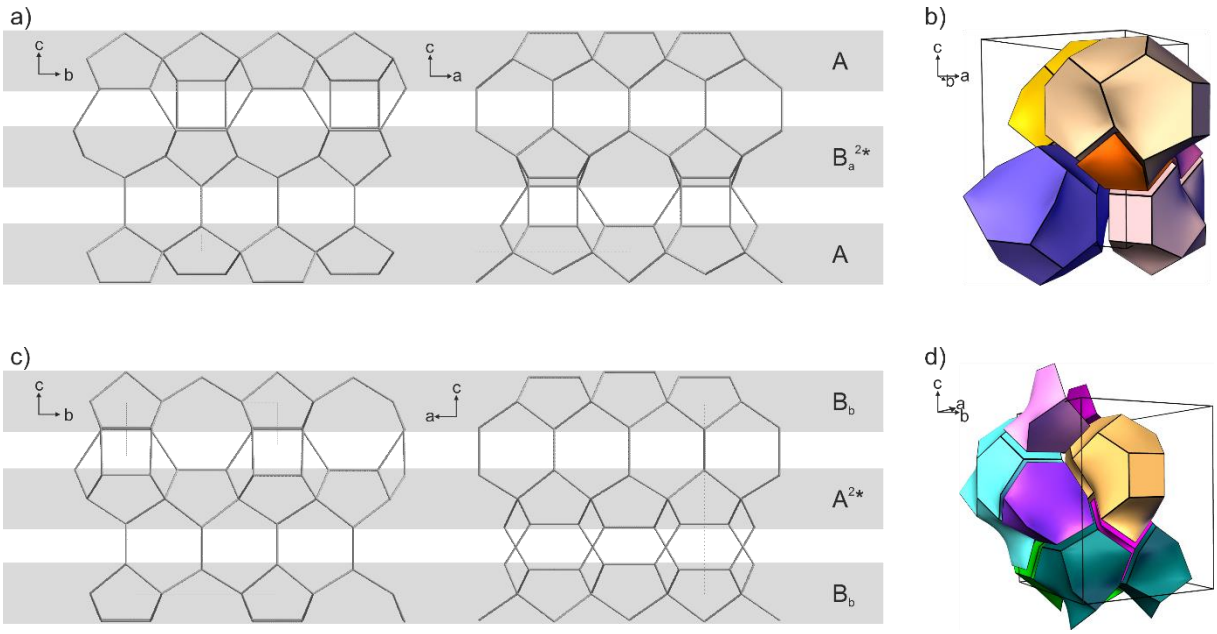

Figure 10**.** Representations of **4** and **5**. a) Parallel projection and stacking sequence of **6**. b) Filling of the unit cell of **4** in terms of natural tiling in $[5^4]$ (orange) + $[5^2.7^2]$ (pink) + $[5^6.6^4.7^2]$ (gold) + $[5^4.6^4.7^4]$ (dark blue) + 2 $[4^2.5^8.6^4]$ (bronze and rose) polyhedra. c) Parallel projection and stacking sequence of **5**. d) Filling or the unit cell of **5** in terms of natural tiling in $[5^4]$ (orange) + 4 $[5^2.7^2]$ (rose, pink, violet, and purple) + 4 $[5^2.6^2.7^2]$* (dark and light green) + $[5^4.6^4.7^4]$ (turquoise, note: its faces are differently arranged than in structure **4**) + $[4^2.5^8.6^4]$ (bronze).

jfk3 (6). Stacking of layers A and C^1 leads to structure **6**. The network with space group $P\bar{4}$ (81) is built by five symmetry independent Si positions per unit cell (Figure 11a). Its natural tiling is $2[8^3] + [5^4] + 10[5^2.8^2]$ (Figure 11b). It bears a large amount of the helix causing $[5^2.8^2]$ tile (compare reference [7]) and can thus be regarded as a structure with perpendicular and fragmented helices interspersed by realgar units. For connecting the helix fragments of five stacked $[5^2.8^2]$ tiles, a pair of two $[8^3]$ tiles is stacked between them and the opposite end is neighbored by a realgar unit; the $[5^2.8^2]$ tiles occupy three symmetry independent positions in a ratio of 4:4:2 (Figure 11c).

jfk4 (7). The combination of layer C and B_a^4 (B_a is shifted about 0.5, 0.5 against C) forms structure **7**, which can be described in space group *C*222 (21) with 9 symmetry independent Si positions per unit cell (Figure 11d).[45] The natural tiling is $2[8^3] + 3[5^4] + 2[5^2.8^2] + 4[5^2.8^3] + 4[5^6.8^2]$ (Figure 11e). The basic layers for constructing the network are oriented along the diagonals of the resulting unit cell.

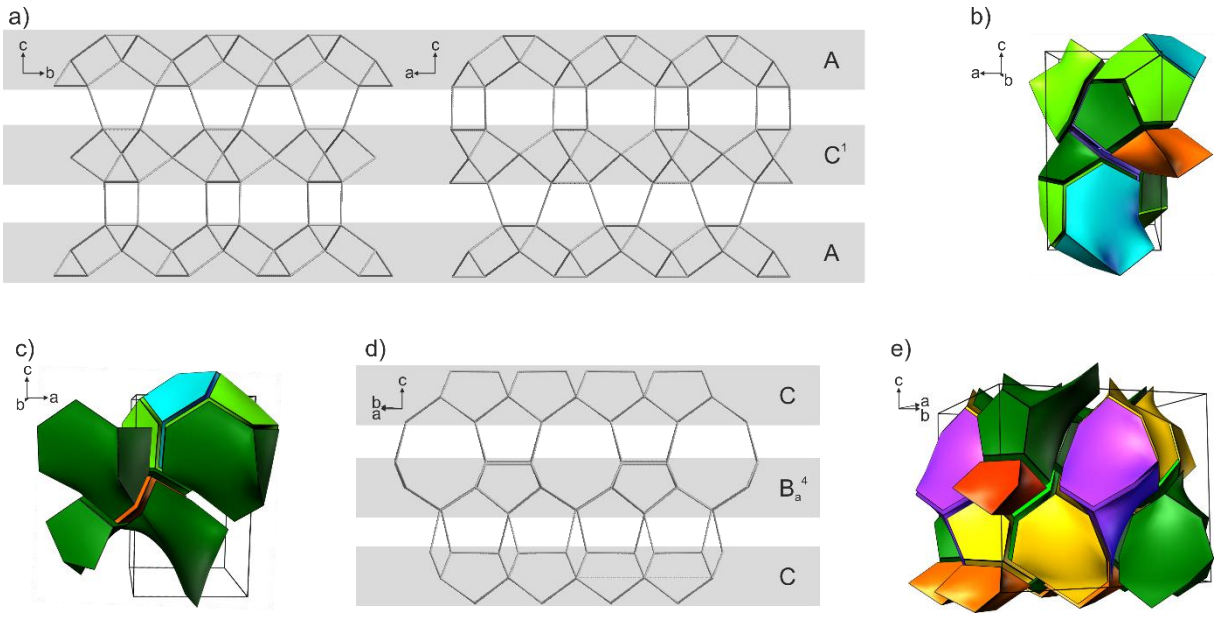

Figure 11**.** Representations of **6** and **7**. a) Parallel projection and stacking sequence of **6**. b) Unit cell of **6** filled in terms of natural tiling in 2[8^3] (purple) + [5^4] (orange) + 10[$5^2.8^2$] (4x dark green, 4x light green, 2x turquoise). c) Surrounding of one realgar unit in **6**; each edge limits a series of five [$5^2.8^2$] tiles that form a helix. The other helix end is limited by a [8^3] tile (not shown). d) Parallel projection and stacking sequence of **7**. e) Unit cell of **7** filled in terms of natural tiling in 2[8^3] (purple) + 3[5^4] (orange and red; the first result from layer C and are symmetry dependent, the latter from layer B_a) + 2[$5^2.8^2$] (green) + 4[$5^2.8^3$] (yellow) + 4[$5^6.8^2$] (forest green).

alt1 (8). Of course, the layer with the highest strain, layer C (Figure 12a) can also be stacked in combination with itself to result in two structures, **alt1** (**8**) and **alt2** (**9**).

Stacking layer C and C^1 results in structure **8**, which can be described in space group *C*222 (21) with three symmetry independent positions per unit cell[46] (Figures 12b and 12c). The natural tiling is 2[8^3] + [5^4] + 4 [$5^2.8^2$] resulting in an average ring size of 6.62, which is the largest ring size of all studied nets (Figure 12d).

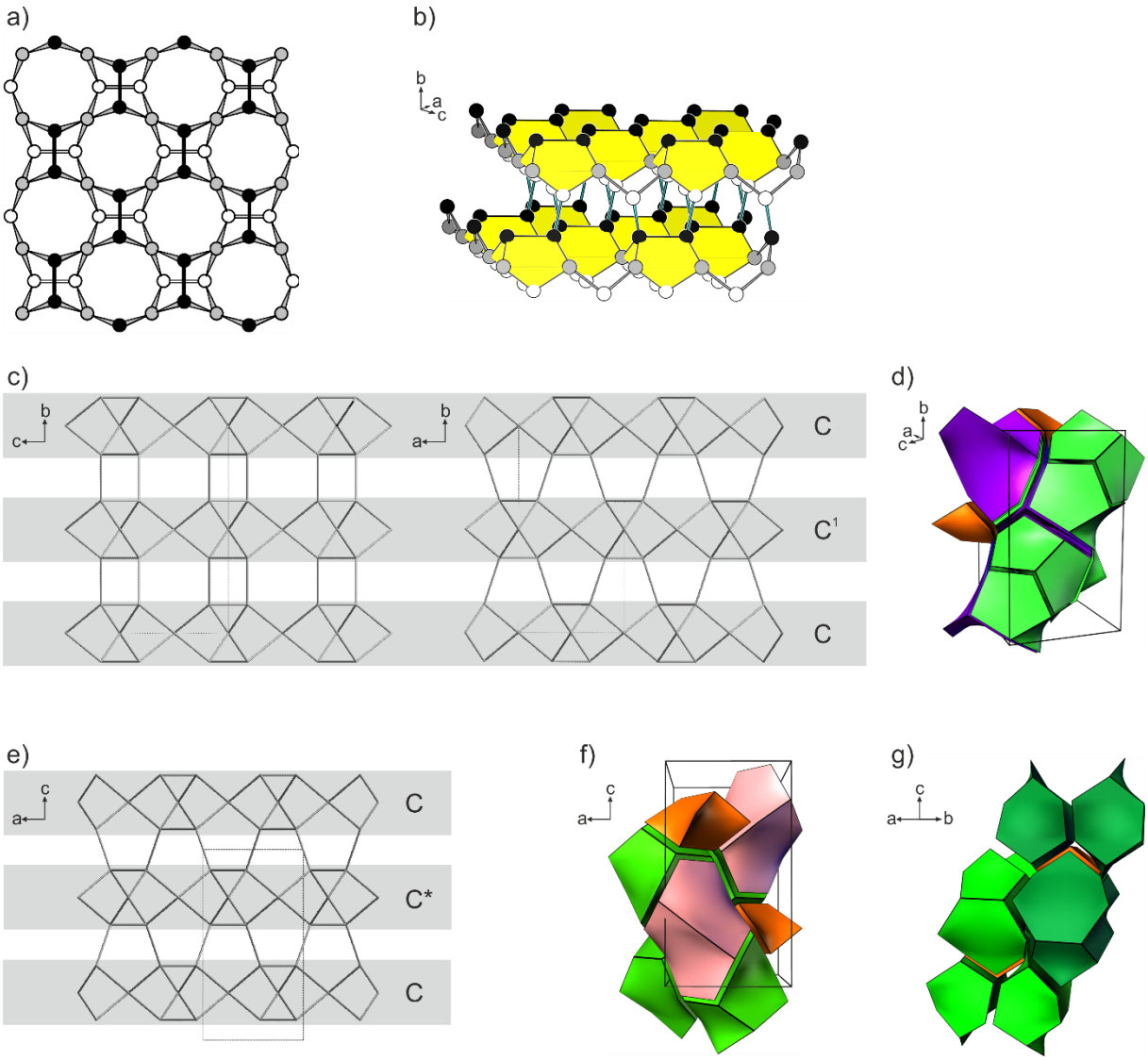

Figure 12. Representations of the two networks **8** and **9** constructed with layer C. a) Layer C. b) Side view of a two-layer stacking C and C^1. c) Parallel projection of structure **8**. Notice: the unit cell of layer C as shown in Figure 1 is rotated by 45° in **8**), d) Unit cell filled in terms of the natural tiling in $2[8^3]$ (purple) + $[5^4]$ (orange) + 4 $[5^2.8^2]$ (green, all symmetry dependent) space filling polyhedra. e) Parallel projection of the two-layer stacking E and E^* of structure **9**. f) Unit cell filled in terms of natural tiling in $[5^4]$ (orange) + $[7^4]$ (rose) + $2[5^2.6^2.7^2]$* (green) polyhedra. g) Arrangement of two unities built of a central $[5^4]$ (orange) and four surrounding $[5^2.6^2.7^2]$* tiles, which are symmetry dependent. The unities – shown in dark and light green – share two faces.

alt2 (9). Structure **9** results from stacking layers C and C^* (Figure 12e). It reveals two symmetry independent Si positions per unit cell and space group $P4_2/nnm$ (134).[47] The tiling of this network is described with $[5^4]$ + $[7^4]$ + $2[5^2.6^2.7^2]$* polyhedra (Figure 12f). Both $[5^2.6^2.7^2]$* tiles are symmetry dependent. It can be described as a regular stacking, where all the realgar units are surrounded by four tiles $[5^2.6^2.7^2]$*, these unities are parallel arranged and share two faces each (Figure 12g, compare above the description for **tum5** in relation to **tum1**).

Si, Ge, and Sn allotropes derived from a set of chemi-inspired structures

In our recent publication [7], we introduced a set of ten Si modifications that are partly already known as sub-structures of binary or ternary Zintl-phases. For a copious study on the allotropes, which bear no realgar units and are thus differently in terms of structural and chemical properties, we also recalculated those for the higher homologues Ge and Sn. All results are shown in Figure 13.

Analyzing the networks with minimal relative energy that bear no realgar units, the energetic order also differs for the elements (Table 3 and Figure 13a). **T12-Si** is preferred over **unj1-Si**, whereas the relative energy of **T12-Ge** and **unj1-Ge** is the same and **unj1-Sn** is preferred over **T12-Sn**. Both considered networks are experimentally accessible; **T12** is known as binary phase CdP_2[48] and **unj1** as the anionic Ga/Sn part structure in $NaGaSn_2$[49] and $NaGaSn_5$[50], the In/Sn network in $NaInSn_2$[51], and the Zn/Sn substructure in *hP*-Na_2ZnSn_5[35]. Thus, network **unj1-Sn** that exists for various substituted Sn frameworks is the minimum structure, whereas the **T12-Si** has the lowest energy for Si and was so far not found as a (substituted) Sn network, but as substituted P network. Based on this finding, we have to distinguish between Si and Sn for estimations on promising candidates of networks that can be found in the various (multinary) phase diagrams.

Considering the relative energies of the Sn modifications, two structures are energetically among the *chemi-inspired* ones, **unj3-Sn** and **unj4-Sn**. Both have a close relation to the experimentally known networks **unj1** and **unj2** (compare the relation between **tum1** and **tum5**, Figure 2) and are quite likely to be found in a way like *tI*-Na_2ZnSn_5 (**unj1**) was identified as high temperature modification of *hP*-Na_2ZnSn_5 (**unj2**).[35] Structurally, the networks without realgar units also only differ slightly with changing elements (Figure 13c–e).

Table 3. Relative energies and band gaps for the three elements Si, Ge and Sn in the modifications **unj1**–**unj4**, **W2**, and **T12**. For detailed structure descriptions, see reference [7].

	E_{rel}/kJ•mol^{-1}			band gap/eV	band gap^{direct}/eV	band gap/eV	band gap^{direct}/eV	band gap/eV	band gap^{direct}/eV
	Si	**Ge**	**Sn**	**Si**		**Ge**		**Sn**	
unj1	7.7	4.6	3.4	3.01	3.46	2.42	2.45	1.76	2.17
unj2	11.1	7.4	5.5	2.62	2.71	2.11	2.45	1.49	1.81
unj3	10.2	6.6	4.8	2.77	2.84	2.18	2.31	1.58	1.69
unj4	8.1	5.6	4.2	2.40	2.90	1.73	2.11	1.25	1.41
W2	15.2	10.9	8.4	2.84	3.17	1.91	2.62	1.29 (d)	-
T12	6.2	4.6	3.5	2.28	3.12	1.50	1.54	0.83	0.86

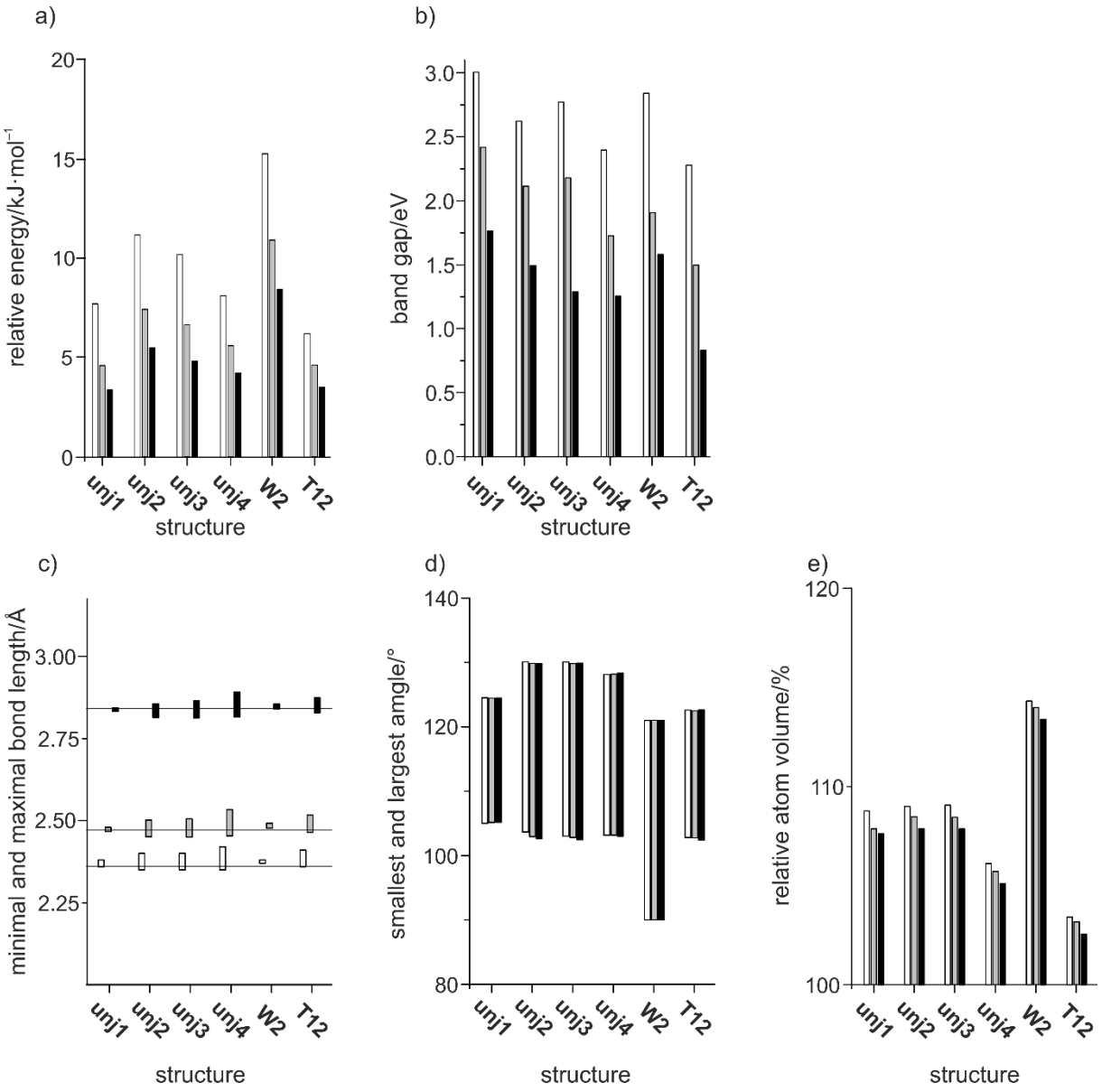

Figure 13. Electronical, structural and topological properties of the networks unj1–unj4, W2, and T12 for the three homologues Si, Ge, and Sn. a) and b) Electronic properties relative energy (compared to the respective α-modification) and bang gap. c)–e) Structural characteristics; minimal and maximal bond lengths (c), range of angles (d), and relative atom volume (e).

Conclusion

We report on a set of nine new three-dimensional tetrahedral Si-networks that show a wide range of relative energy, as we are going to the borders of silicon's structural flexibility. The structures are all systematically derived by rather simple construction rules applied to distorted diamond-structure cutouts allowing for a clear classification. The resulting polytypes are compared to *chemi-inspired* structures, i.e. experimentally appearing frameworks.[7]

At a first glance the construction kit was a simple instruction for use to deriving new structures, but it even more leads to a deep understanding of the relations between the structures as it was highlighted at the example of **tum5** (**1**) and **tum1**, two structures that can be transformed by a smooth atom displacement within the layers. Such a modification was observed for another structure-pair, which is also obtainable with our construction kit,[7] namely **unj1** and **unj2** that both appear in the experimentally established phase transition of Na_2ZnSn_5.[35] Just similar to these two structures, **tum5** could be found as substructures in compounds in the phase systems Li/B/Si, Na/Zn/Sn or Na/Hg/Sn crystallizing with the anionic **tum1** partial structure.[36-37] Additional, both have a structural motifs that is also found in **pbam**,[23b] which we analyzed in larger context in this work.

As several structures are experimentally found as substituted Sn networks, we expanded our computational study to the higher homologues Ge and Sn which reveals interesting trends within the homologues by inspecting the total energies relative to the respective diamond structures. With this finding, we were able to distinguish between networks that are in the range of experimentally accessible structures for substituted Si and Sn networks. Further, we elucidated the changes in band structures in dependency of the considered element. Network **tum5-Si** is a semiconductor with indirect band gap, **tum5-Ge** in contrast bears a direct band gap and **tum5-Sn** is metallic with touching band. This comes along with a large difference in relative energies for **tum5-Si**, **tum5-Ge** and **tum5-Sn**.

Some of the modifications discussed throughout this work additionally include special structural features as channels or large cavities, making them interesting for intercalation materials, which could be synthesized by a phase transition, as they are so closely related to accessible structures and not only found *in silico*.

Acknowledgements

The authors thank for support through the research network “Solar Technologies go Hybrid” (State of Bavaria) via TUM.solar.

Notes and references

[1] W. Bludau, A. Onton, W. Heinke, *J. Appl. Phys.* **1974**, *45*, 1846-1848.

[2] K. Sun, S. Shen, Y. Liang, P. E. Burrows, S. S. Mao, D. Wang, *Chem. Rev.* **2014**, *114*, 8662-8719.

[3] B. Li, X. Gao, J. Li, C. Yuan, *Environ. Sci. Techn.* **2014**, *48*, 3047-3055.

[4] a) W.-J. Zhang, *J. Power Sources* **2011**, *196*, 13-24; b) Z. L. Hu, S. Zhang, C. J. Zhang, G. L. Cui, *Coord. Chem. Rev.* **2016**, *326*, 34-85; c) T. D. Bogart, A. M. Chockla, B. A. Korgel, *Curr. Op. Chem. Eng.* **2013**, *2*, 286-293.

[5] a) N. A. Wagner, R. Raghavan, R. Zhao, Q. Wei, X. Peng, C. K. Chan, *Chem. Electro. Chem.* **2014**, *1*, 347-353; b) T. Langer, S. Dupke, H. Trill, S. Passerini, H. Eckert, R. Pöttgen, M. Winter, *J. Electrochem. Soc.* **2012**, *159*, A1318-A1322; c) M. Beekman, K. Wei, G. S. Nolas, *Appl. Phys. Rev.* **2016**, *3*, 040804.

[6] M. Zeilinger, L.-A. Jantke, L. M. Scherf, F. J. Kiefer, G. Neubüser, L. Kienle, A. J. Karttunen, S. Konar, U. Häussermann, T. F. Fässler, *Chem. Mater.* **2014**, *26*, 6603-6612.

[7] L. A. Jantke, S. Stegmaier, A. J. Karttunen, T. F. Fässler, *Chem. Eur J.* **2017**, *23*, 2734-2747.

[8] M. Beekman, *Mater. Today* **2015**, *18*, 304-305.

[9] a) C. He, C. Zhang, J. Li, X. Peng, L. Meng, C. Tang, J. Zhong, *Phys. Chem. Chem. Phys.* **2016**, *18*, 9682-9686; b) Q. Fan, C. Chai, Q. Wei, Y. Yang, *Phys. Chem. Chem. Phys.* **2016**; c) M. Amsler, S. Botti, M. A. L. Marques, T. J. Lenosky, S. Goedecker, *Phys Rev B* **2015**, *92*; d) S. Botti, J. A. Flores-Livas, M. Amsler, S. Goedecker, M. A. L. Marques, *Phys Rev B* **2012**, *86*; e) Q. Zhu, A. R. Oganov, A. O. Lyakhov, X. X. Yu, *Phys Rev B* **2015**, *92*.

[10] P. Norouzzadeh, C. W. Myles, D. Vashaee, *Sci. Rep.* **2014**, *4*.

[11] V. J. Härkönen, A. J. Karttunen, *Phys Rev B* **2016**, *93*, 4307-4307.

[12] a) A. M. Guloy, R. Ramlau, Z. Tang, W. Schnelle, M. Baitinger, Y. Grin, *Nature* **2006**, *443*, 320-323; b) A. Ammar, C. Cros, M. Pouchard, N. Jaussaud, J.-M. Bassat, G. Villeneuve, M. Duttine, M. Ménétrier, E. Reny, *Solid State Sci.* **2004**, *6*, 393-400.

[13] S. Wippermann, Y. P. He, M. Voros, G. Galli, *Appl. Phys. Rev.* **2016**, *3*.

[14] A. Marzouk, P. B. Balbuena, F. El-Mellouhi, *Electrochim. Acta* **2016**, *207*, 301-307.

[15] a) M. A. Zwijnenburg, K. E. Jelfs, S. T. Bromley, *Phys. Chem. Chem. Phys.* **2010**, *12*, 8505-8512; b) K. Luo, Z. S. Zhao, M. D. Ma, S. S. Zhang, X. H. Yuan, G. Y. Gao, X. F. Zhou, J. L. He, D. L. Yu, Z. Y. Liu, B. Xu, Y. J. Tian, *Chem. Mater.* **2016**, *28*, 6441-6445; c) Q. Fan, C. Chai, Q. Wei, H. Yan, Y. Zhao, Y. Yang, X. Yu, Y. Liu, M. Xing, J. Zhang, R. Yao, *J. Appl. Phys.* **2015**, *118*.

[16] a) Z. Zhao, F. Tian, X. Dong, Q. Li, Q. Wang, H. Wang, X. Zhong, B. Xu, D. Yu, J. He, H.-T. Wang, Y. Ma, Y. Tian, *J. Am. Chem. Soc.* **2012**, *134*, 12362-12365; b) Q. Wang, B. Xu, J. Sun, H. Liu, Z. Zhao, D. Yu, C. Fan, J. He, *J. Am. Chem. Soc.* **2014**, *136*, 9826-9829.

[17] M. C. Nguyen, X. Zhao, C.-Z. Wang, K.-M. Ho, *Phys Rev B* **2014**, *89*, 184112.

[18] a) Q. Y. Fan, C. C. Chai, Q. Wei, P. K. Zhou, J. Q. Zhang, Y. T. Yang, *Materials* **2016**, *9*; b) Y. Guo, Q. Wang, Y. Kawazoe, P. Jena, *Sci. Rep.* **2015**, *5*.

[19] a) R. Hoffmann, A. A. Kabanov, A. A. Golov, D. M. Proserpio, *Angew. Chem. Int. Ed.* **2016**, *55*, 10962-10976; b) I. A. Baburin, D. M. Proserpio, V. A. Saleev, A. V. Shipilova, *Phys. Chem. Chem. Phys.* **2015**, *17*, 1332-1338.

[20] M. O'Keeffe, G. B. Adams, O. F. Sankey, *Philosoph. Mag. Lett.* **1998**, *78*, 21-28.

[21] I. H. Lee, Y. J. Oh, S. Kim, J. Lee, K. J. Chang, *Comp. Phys. Commun.* **2016**, *203*, 110-121.

[22] a) V. L. Deringer, G. Csanyi, D. M. Proserpio, *ChemPhysChem* **2017**. b) R. Nesper, K. Vogel, P. E. Blochl, A*ngew. Chem. Int. Ed. Engl.* **1993**, *32*, 701–703; *Angew. Chem.* **1993**, *105*, 786–788.

[23] a) Y. J. Oh, I. H. Lee, S. Kim, J. Lee, K. J. Chang, *Sci. Rep.* **2015**, *5*; b) A. Mujica, C. J. Pickard, R. J. Needs, *Phys Rev B* **2015**, *91*.

[24] a) L. Rapp, B. Haberl, C. J. Pickard, J. E. Bradby, E. G. Gamaly, J. S. Williams, A. V. Rode, *Nat. Commun.* **2015**, *6*; b) D. Y. Kim, S. Stefanoski, O. O. Kurakevych, T. A. Strobel, *Nat. Mater.* **2015**, *14*, 169-173.

[25] a) Q. Fan, C. Chai, Q. Wei, Y. Yang, Q. Yang, P. Chen, M. Xing, J. Zhang, R. Yao, *J. Solid State Chem.* **2016**, *233*, 471-483; b) Q. Y. Fan, C. C. Chai, Q. Wei, Q. Yang, P. K. Zhou, M. J. Xing, Y. T. Yang, *Mater. Sci. Semicond. Process.* **2016**, *43*, 187-195.

[26] R. Dovesi, R. Orlando, B. Civalleri, C. Roetti, V. R. Saunders, C. M. Zicovich-Wilson, *Z. Kristallogr.* **2005**, *220*, 571-573.
[27] J. P. Perdew, K. Burke, M. Ernzerhof, *Phys. Rev. Lett.* **1996**, *77*, 3865-3868.
[28] A. J. Karttunen, T. F. Fässler, M. Linnolahti, T. A. Pakkanen, *Inorg. Chem.* **2011**, *50*, 1733-1742.
[29] H. T. Stokes, D. M. Hatch, *J. Appl. Cryst.* **2005**, *38*, 237-238.
[30] C. Adamo, V. Barone, *J. Chem. Phys.* **1999**, *110*, 6158-6170.
[31] a) F. Pascale, C. M. Zicovich-Wilson, F. López Gejo, B. Civalleri, R. Orlando, R. Dovesi, *J. Comput. Chem.* **2004**, *25*, 888-897; b) C. M. Zicovich-Wilson, F. Pascale, C. Roetti, V. R. Saunders, R. Orlando, R. Dovesi, *J. Comput. Chem.* **2004**, *25*, 1873-1881.
[32] Y. Yang, Y. Hwang, H. A. Cho, J.-H. Song, S.-J. Park, J. A. Rogers, H. C. Ko, *Small* **2011**, *7*, 484-491.
[33] a) V. A. Blatov, O. Delgado-Friedrichs, M. O'Keeffe, D. M. Proserpio, *Acta Cryst. A* **2007**, *63*, 418-425; b) M. O'Keeffe, B. G. Hyde, *Crystal Structures, I. Patterns and Symmetry*, Mineralogical Society of America, Washington, **1996**.
[34] V. A. Blatov, *Struct. Chem.* **2012**, *23*, 955-963.
[35] S. Stegmaier, S.-J. Kim, A. Henze, T. F. Fässler, *J. Am. Chem. Soc.* **2013**, 10654–10663.
[36] M. Zeilinger, L. van Wüllen, D. Benson, V. F. Kranak, S. Konar, T. F. Fässler, U. Häussermann, *Angew. Chem. Int. Ed.* **2013**, *52*, 5978-5982.
[37] S. Ponou, S.-J. Kim, T. F. Fässler, *J. Am. Chem. Soc.* **2009**, *131*, 10246-10252.
[38] The *initial 4b*-Si occupy Wyckoff position 8*l*.
[39] The two $[5^2.6^2.7^2]$ tiles are symmetry dependent and the two $[5^2.6^2.7^2]$* tiles not.
[40] Note that only one sort of the two symmetry independent $[5^2.6^2.7^2]$* tiles (green in Figures 3d and f) is sharing a face with $[5^4]$.
[41] W. Setyawan, S. Curtarolo, *Comput. Mater. Sci.* **2010**, *49*, 299-312.
[42] Note: Due to the rule of forming strong rings, our networks may show large and partly obtuse tiles.
[43] Also **6-Si** and **6-Sn** show a narrow range of all distances except for one bond type: the bonds above and below the plane trough the *initial 4b* atoms completing the realgar units of layer C are longer.
[44] All are situated at Wyckoff position 2*a*.
[45] The *initial 4b*-Si atoms are located at Wyckoff positions 2*a*, 2*b*, 4*h*, 4*f*, and 4*k*.
[46] The *initial 4b*-Si are situated at Wyckoff positions 2*a* and 2*c* and all newly connected Si atoms are at Wyckoff position 8*l*.
[47] The *initial 4b*-Si atoms are situated at Wyckoff position 4*c* and all newly connected Si atoms at Wyckoff position 8*m*.
[48] a) J. Goodyear, G. A. Steigmann, *Acta Cryst. B* **1969**, *B25*, 2371-2374; b) J. Berak, Z. Pruchnik, *Roczniki Chemii* **1969**, *43*, 1141-&; c) O. Olofsson, J. Gullman, *Acta Cryst. B* **1970**, *B 26*, 1883-&; d) Both, the α- and the β- modification show the topology of **T12**, they are just differently distorted.
[49] J. T. Vaughey, J. D. Corbett, *J. Am. Chem. Soc.* **1996**, *118*, 12098-12103.
[50] W. Blase, G. Cordier, *Z. Naturforsch. B* **1988**, *43*, 1017-1019.
[51] W. Blase, G. Cordier, *Z. Naturforsch. B* **1989**, *44*, 1479-1482.